The Journal of Adhesion

ISSN: 0021-8464 (Print) 1545-5823 (Online) Journal homepage: https://www.tandfonline.com/loi/gadh20

Study on the structural parameters and adhesive force of gecko seta

Q. K. Zhang & L. X. Li

To cite this article: Q. K. Zhang & L. X. Li (2019): Study on the structural parameters and adhesive force of gecko seta, The Journal of Adhesion, DOI: 10.1080/00218464.2019.1615466

To link to this article: https://doi.org/10.1080/00218464.2019.1615466

Published online: 14 May 2019.

THE JOURNAL OF ADHESION
https://doi.org/10.1080/00218464.2019.1615466

Taylor & Francis
Taylor & Francis Group

Study on the structural parameters and adhesive force of gecko seta

Q. K. Zhang and L. X. Li

State Key Laboratory for Strength and Vibration of Mechanical Structures, Shaanxi Key Laboratory of Environment and Control for Flight Vehicle, School of Aerospace Engineering, Xi'an Jiaotong University, Xi'an, Shaanxi, PR China

ABSTRACT

It is found from the observation that seta on the adhesive pad of gecko is around several microns in diameter and has a multilevel projective terminal which eventually forms 100 ~ 1000 projections. In addition, the adhesive force of a single seta is about 20 ~ 200μN. To explain this fine structure and such a large adhesive force of seta, we develop an ideal-self-similar hierarchical model composed of a fiber array at each level to mimic the multilevel projective terminal of single gecko's seta. With this model, the variations of the properties with increasing number of levels are investigated. For Tokay gecko's seta, the total number of levels is first estimated, and the structural parameters such as radius, the total number of terminal fibers and the adhesive force are then predicted. The results agree well with those observed in nature. Furthermore, with the present model, the dominant failure mode of each level is always the adhesion failure, and the role of structural hierarchy for adhesion release is addressed.

ARTICLE HISTORY
Received 13 January 2019
Accepted 2 May 2019

KEYWORDS
Biomechanics; hierarchical material; ideal-self-similarity; fiber array; flaw tolerant adhesion; seta

1. Introduction

In nature, fine structure and large adhesive force are the prevailing features that can be observed in many biological adhesive systems.[1–4] Among them, gecko has exceptional ability to climb rapidly up vertical walls and ceilings which have unpredictable rough surfaces.[5] However, current man-made materials cannot achieve this ability. Microscopy[6,7] has shown that the gecko's foot possesses nearly five millions keratinous setae, and each seta (Figure 1a) is 30 ~ 130 μm in length and several microns in diameter with a multilevel projective terminal which eventually forms hundreds of projections. Figure 1b is the schematic diagram of a single seta. It can be seen that the projections of each level in multilevel projective terminal form a fiber array. In addition, previous studies[11–13] have provided evidence that the robust adhesion of gecko is primarily due to the van der Waals interaction

CONTACT L. X. Li luxianli@mail.xjtu.edu.cn State Key Laboratory for Strength and Vibration of Mechanical Structures, Shaanxi Key Laboratory of Environment and Control for Flight Vehicle, School of Aerospace Engineering, Xi'an Jiaotong University, Xi'an, Shaanxi 710049, PR China

Color versions of one or more of the figures in the article can be found online at www.tandfonline.com/gadh.

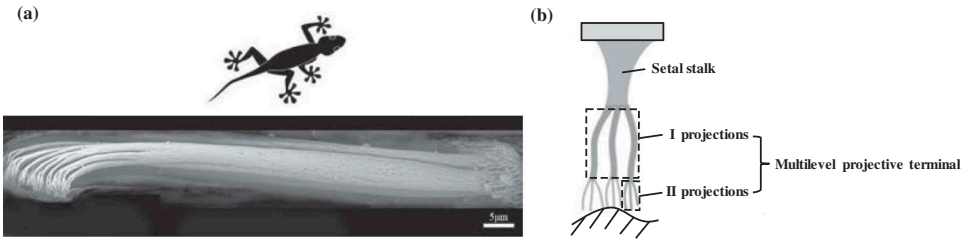

Figure 1. Multilevel design of gecko seta: (a) SEM of a single seta which has a multilevel projective terminal[8,9]; (b) The schematic diagram of a single seta (based on the reference[10] with some modifications). The projections of each level in multilevel projective terminal form a fiber array.

between the contact surfaces and the gecko's feet, namely, dry adhesion; and obtained that the adhesive force is around 20 ~ 200μN for a single seta. A question of interest is how nature designs the fine structure and generates the large adhesive force for gecko seta.

In the past 20 years, much attention has been paid to the adhesive mechanisms of gecko,[9,13–15] as well as the properties of a single seta,[8,16,17] and the setal array.[18–20] In contrast, the multilevel models were widely adopted to study the structural parameters (i.e. radius, the total number of terminal fibers) and the adhesive force of gecko seta, including the three-levels model of spatula, seta and toe,[21,22] the self-similar hierarchical model of seta and setal array,[10,23,24] and the computational combined hierarchical model of seta and spatula.[25,26] However, the fine structure and the large adhesive force of a single seta cannot be interpreted in a consistent manner. For example, the three-levels model[21] could well predict the diameter of seta, but the predicted adhesive force was only twentieth to one-half of the observations. Furthermore, this model does not consider the hierarchical effect in seta which is crucial to the multilevel projective terminal. In the self-similar hierarchical model,[23] the structural parameters and adhesive force of seta can be all predicted, but the predicted total number of levels was much lower than the observations. Meanwhile, the predicted results significantly deviated from the experimental observations for the total number of levels (i.e. level 3) if fibers are placed in a hexagonal pattern. For the computational combined hierarchical model,[26] the geometric modeling was proposed in close accordance with the structural parameters of seta, but the calculated adhesive force was much lower than the observations.

To overcome the above-mentioned shortcomings, an ideal-self-similar hierarchical model is developed in this paper to mimic the multilevel projective terminal of a single seta. With this model, the gap between the theoretical predictions and the observations about the structural parameters and adhesive force of seta is addressed. Meanwhile, the present model

remains the robust adhesion for each level and helps to reveal the role of structural hierarchy for adhesion release of seta.

2. Derivation of the model

2.1. *The ideal-self-similar hierarchical model*

Observations[6,7] show that the multilevel projective terminal of gecko seta is composed of several levels, and eventually forms hundreds of projections. It indicates that the number of projections at each level is only a single digit for this hierarchical structure. On the other hand, the number of setae in one toe is in the order of one million with approximately 14400 setae per square millimeter.[12,27] Thus, a single seta has a quite different hierarchical manner from the setal array in toe. Based on this fact, our focus is on modeling the multilevel projective terminal of a single seta.

Considering the optimal evolution of biological structures, an ideal-self-similar hierarchical model is proposed to describe the multilevel projective terminal of a single seta, as shown in Figure 2. In this model, each level is a fiber array which can be regarded as a complete structure. In the array, every fiber has a terminal which consists of the smaller fiber array at the lower level (except for level 0), and the aggregation of the terminals of all fibers in the array forms the array's terminal. Meanwhile, it is assumed that the array has the same number of fibers, and the two adjacent levels have the same size ratios. That is,

$$m_n = m,\ n = 1, 2, 3, \ldots, \tag{1}$$

$$R_n / R_{n-1} = c_1, \tag{2}$$

and

$$L_n / L_{n-1} = c_2, \tag{3}$$

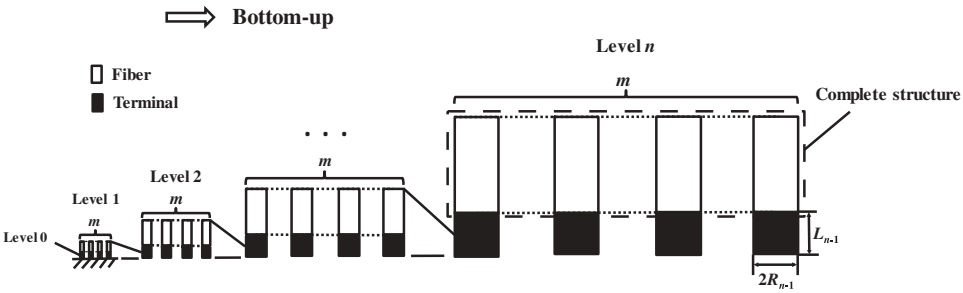

Figure 2. The ideal-self-similar hierarchical model for the multilevel projective terminal of gecko seta based on the bottom-up design[10,23]: "ideal" means each level is an array with the same number of fibers (i.e. $m_n = m$) and the two adjacent levels have the same size ratios; "self-similar " means the terminal of fiber at a level is composed of the smaller fiber array at the lower level.

where R_n and L_n represent the radius and length of level n, m represents the number of fibers in the fiber array, while c_1 and c_2 denote two constants. In this paper, m, c_1 and c_2 are called structural constants.

With the radius and the number of fibers, the area fraction of fibers at level n is expressed as

$$\varphi_n = mR_{n-1}^2/R_n^2 = m/c_1^2 = \varphi. \tag{4}$$

Equation (4) indicates that each level also has the same area fraction of fibers φ in the present model.

2.2. *The sizes based on the flaw tolerant adhesion*

Because seta has the robust dry adhesion, the sizes of each level are constructed by using the flaw tolerant adhesion. In an adhesion problem, the state of flaw tolerance is considered to be a pre-existing crack (an interfacial crack is used to simulate the random contact flaws induced by roughness or contaminants) which, for any size and orientation, does not propagate during the failure process. The failure occurs when the normal traction reaches the theoretical adhesion strength everywhere along with the interface except for the region occupied by the crack.[28,29] Thus, because of the reach of the theoretical adhesion strength, the simultaneous detachment of the whole contacting area rather than the crack propagation causes the interface failure.

The critical condition for the fiber array at level n to remains flaw tolerant adhesion is that the radius R_n should satisfy[23]

$$R_n = \frac{8E_nW_n}{\pi(1-\nu^2)S_n^2}, \quad n = 0,\ 1,\ 2, \ldots, \tag{5}$$

where E_n, S_n and W_n denote the Young's modulus, adhesion strength and work of adhesion at the n-th level, respectively. It should be noted that, because the structure of fiber array at each level in the present model is different from that of a single fiber in the self-similar hierarchical model,[23] Young's modulus of each level in the self-similar hierarchical model,[23] i.e. E_f, is replaced by E_n in Equation (5). Meanwhile, ν is the Poisson's ratio of the fiber array and assumed constant at each level.

Actually, an adhesion material can tolerate the interfacial flaw whose size is no more than the critical value.[29] Thus, the condition to achieve flaw tolerant adhesion[14] can be taken to be that the characteristic size of the material is less than or equal to the critical size of crack. Since the size of crack has a conjugate opening displacement, the characteristic size of material will also have a conjugate characteristic length (see Appendix A for the derivation).

For the radius R_n in Equation (5), the conjugated length L_n at level n is therefore expressed as

$$L_n = \frac{2(1-\nu)E_n W_n}{(1+\nu)(1-2\nu)S_n^2}. \tag{6}$$

With Equations (5) and (6), the length-diameter ratio of each level is expressed by $L_n/(2R_n) = \pi(1-\nu)^2/[8(1-2\nu)]$. For the values of $m = 5$ and $\nu = 0.1 \sim 0.4$, the length-diameter ratio is 1.99 ~ 3.54 for a single fiber at each level. Though the values of the length-diameter ratio are smaller than that of seta, i.e. 6 ~ 26,[6,7] it is still acceptable for the multilevel projective terminal we are studying. In addition, for these short fibers, the bundling effect of the neighboring fibers can be ignored.

2.3. *Properties at each level*

First, we study the material properties (i.e. E_n, S_n and W_n) at each level.

To this end, the adhesion problem is examined for each level. As shown in Figure 3, the adhesion occurs through contacting of the array's terminal (regarded as a cohesive layer) with the substrate. Thus, the material properties of the fiber array at each level should be characterized by those of the array's terminal in an effective sense.

Thus, the effective Young's modulus of level n has a recursively relation as

$$E_n = \varphi E_{n-1} \text{ with } E_0 = E_f, \quad n = 1, 2, 3, \ldots, \tag{7}$$

where E_f is the Young's modulus of fiber.

Similarly, the effective adhesion strength of level n expresses as

$$S_n = \varphi S_{n-1} \text{ with } S_0 = \sigma_{th} \tag{8}$$

where σ_{th} is the theoretical strength of van der Waals interaction.

Because the elastic deformation of the array's terminal will make a significant contribution to the separation process for the fiber array in the flaw tolerant adhesion,[23] an energy dissipation term ΔW_{n-1} must be added to the effective work of adhesion of level n as

$$W_n = (W_{n-1} + \Delta W_{n-1})\varphi \text{ with } W_0 = \Delta\gamma, \tag{9}$$

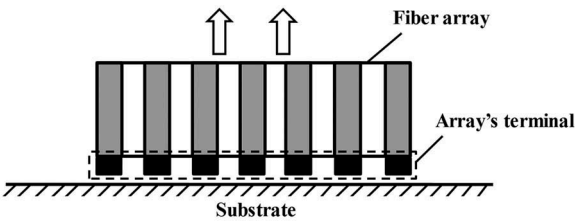

Figure 3. Adhesion of each level: contact of the array's terminal with the substrate.

where $\Delta\gamma$ is the van der Waals energy of fiber.

From the elasticity theory and Equation (6), it is not difficult to obtain

$$\Delta W_{n-1} = \frac{S_{n-1}^2 L_{n-1}}{2E_{n-1}} = \frac{(1-\nu)}{(1+\nu)(1-2\nu)} W_{n-1}. \tag{10}$$

With Equation (10), Equation (9) yields

$$W_n = \nu^* \varphi W_{n-1} \text{ with } \nu^* = \frac{2(1-\nu-\nu^2)}{(1+\nu)(1-2\nu)} \tag{11}$$

With Equations (7), (8) and (11), constant c_1 is identified as

$$c_1 = R_n/R_{n-1} = \nu^* \tag{12}$$

from Equation (5) and constant c_2 is identified as

$$c_2 = L_n/L_{n-1} = \nu^* = c_1 \tag{13}$$

from Equation (6).

Upon Equations (4), we further obtain

$$E_n/E_0 = \left(m/c_1^2\right)^n \tag{14}$$

from Equation (7) and

$$S_n/S_0 = \left(m/c_1^2\right)^n \tag{15}$$

from Equation (8).

Upon Equations (4) and (12), we obtain

$$W_n/W_0 = (m/c_1)^n \tag{16}$$

from Equation (11).

Equations (14), (15) and (16) are the effective material properties of each level relative to those of level 0. It is seen that the three effective material properties are governed by the two structural constants m and c_1.

While c_1 is calculated from the Poisson's ratio, m can be calculated by following the geometrical admissible placement of fibers. This means that m cross-sections with radius R_{n-1} must be completely placed in a cross-section with radius R_n. If a regular lattice pattern is assumed, from the derivation in Appendix B, we obtain the requirement for m as

$$3 \le m \le \pi/\arcsin\left(\frac{1}{c_1-1}\right) \text{ with } c_1 \ge 2.154 \tag{17}$$

Next, we study other properties of each level.

As the two structural parameters, the total number of terminal fibers M_n and radius R_n can be cast as

$$M_n = \prod_{i=1}^{n} m_i = m^n \tag{18}$$

from Equation (1) and

$$R_n/R_0 = c_1^n \tag{19}$$

from Equation (2).

For the conjugated length L_n relative to radius, Equation (3) yields

$$L_n/L_0 = c_1^n. \tag{20}$$

With the knowledge of the radius and adhesion strength, the adhesive force of level n can be calculated by

$$F_n = \pi R_n^2 S_n \quad \text{with} \quad F_0 = \pi R_0^2 S_0 \tag{21}$$

From Equations (15) and (19), we further obtain

$$F_n/F_0 = (R_n/R_0)^2 (S_n/S_0) = m^n. \tag{22}$$

3. Results

3.1. *Variations of the properties in the ideal-self-similar hierarchical model*

With the derivations in Section 2, variations of the properties in the ideal-self -similar hierarchical model with the number of levels can be studied. To this end, we first determine the structural constants.

Consider the fact of $\nu = 0.3$ for the keratin of seta,[23] two values of $\nu = 0.3$ and $\nu = 0.35$ are, respectively, examined for the Poisson's ratio of fiber array. The structural constants are calculated from Equations (12), (13) and (17), together with the area fraction φ from Equation (4), as listed in Table 1. It is seen that c_1 satisfies Equation (17) for the two cases, and m can be taken 3 or 4 for the case of $\nu = 0.35$.

Then, the properties at different levels are calculated by using the ideal-self -similar hierarchical model, as shown in Figure 4.

Figure 4a-b plot the variations of the three material properties as a function of level n. From Figure 4a, it is seen that the Young's modulusE_n and adhesion strength S_n have the same dimensionless values at each level

Table 1. The structural constants and area fraction for the ideal-self-similar hierarchical model.

	$\nu = 0.3$	$\nu = 0.35$	
$c_1 = c_2$	2.346	2.605	
m	3	3	4
φ	0.545	0.442	0.589

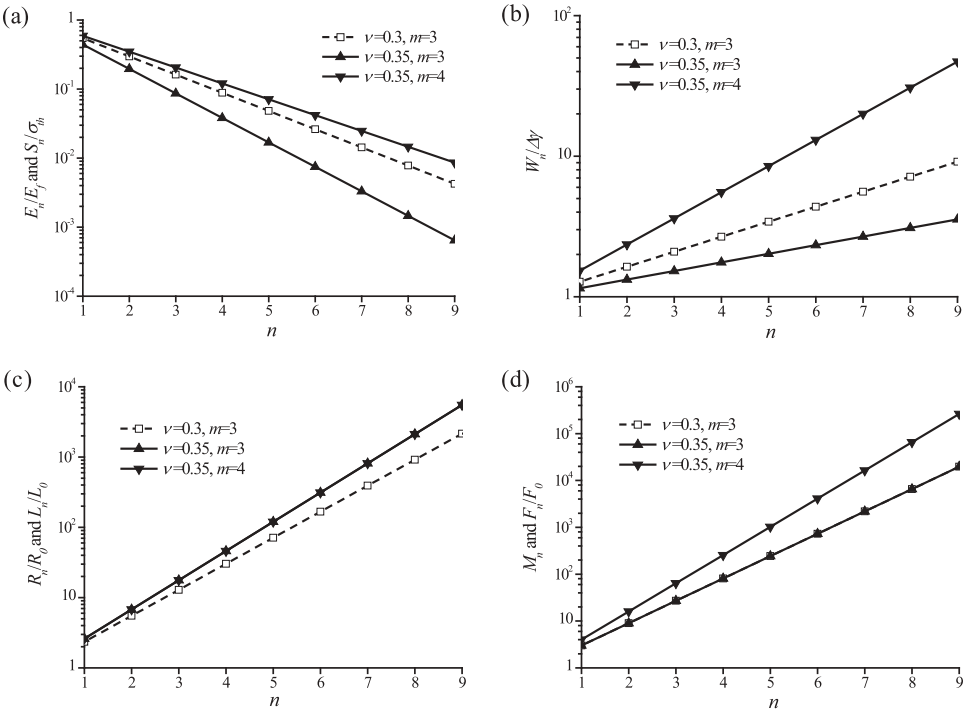

Figure 4. Variations of (a) the Young's modulus and adhesion strength, (b) the work of adhesion, (c) the radius and length, and (d) the total number of terminal fibers and adhesive force with level *n*.

relative to those of level 0, which decrease exponentially with increasing the number of levels. Meanwhile, Figure 4a shows $E_n/E_f < 1$, which indicates the hierarchical structure behaves softer than the straight structure. As pointed out in references,[30–32] the decrease of rigidity is beneficial to increasing the adhesion ability of seta, and therefore physically reasonable. From Figure 4b, it is seen that the work of adhesion W_n increases exponentially as the level number increases, which is different from the other two material properties. In addition, the three material properties are all dependent on the number of fibers m as well.

Figure 4c-d plot the variations of the other properties as a function of level n. It is seen that radius R_n, length L_n, the total number of terminal fibers M_n and the adhesive force F_n have the same tendency as W_n shown in Figure 4b. Meanwhile, R_n and L_n have the same dimensionless values at each level relative to those of level 0, and the values when $\nu = 0.3$ are smaller than those when $\nu = 0.35$. Interestingly, by comparing Equations (22) with (18), the dimensionless value of the adhesive force is found to be the total number of fibers at each level. On the whole, a bigger Poisson's ratio of the array leads to larger sizes, and more fibers at each level generate a larger adhesive force.

3.2. *Predictions of the structural parameters and adhesive force of gecko seta*

In this section, we study the structural parameters and adhesive force of Tokay gecko's seta. First, the values of the properties at level 0 are determined. Taking the material properties of keratin as $E_f = E_0 = 1\text{GPa}$, $\sigma_{th} = S_0 = 20\text{MPa}$, $\Delta\gamma = W_0 = 10\text{mJ/m}^2$,[23] the radius, length and adhesive force of level 0 are calculated from Equations (5), (6) and (21) respectively, as listed in Table 2.

Next, we determine the total number of hierarchical levels. Regarding the radius of seta R_{seta} as R_N and the radius of spatula stalk $R_{\text{spatula stalk}}$ as R_0, the total number of hierarchical levels N can be estimated from Equation (19) by

$$N = \frac{\ln(R_{\text{seta}}/R_{\text{spatula stalk}})}{\ln c_1}. \tag{23}$$

For Tokay gecko's seta, we have $R_{\text{seta}} = 2.5\mu\text{m}$[6,7,12], and $R_{\text{spatula stalk}} = 50 \sim 100n\text{m}$.[23] From Equation (23), N should be 3.775 ~ 4.588 for $\nu = 0.3$ and 3.362 ~ 4.086 for $\nu = 0.35$, respectively. It is seen that $N = 4$ is probably reasonable.

Finally, the structural parameters and adhesive force of Tokay gecko's seta are predicted. From Equation (18), (19) and (22), they are obtained, as compared with the observations of gecko seta in Table 3. It is seen that the radius of seta is $2.121\mu\text{m}$ when $\nu = 0.3$ and $3.342\mu\text{m}$ when $\nu = 0.35$, both the two predicted values are close to $2.5\mu\text{m}$ from observations.[6,7,12] For the total number of fibers, the predicted value is 81 when $m = 3$ and 256 when $m = 4$. Compared with the interval of 100 ~ 1000 from observation,[11,12,34] the first value (i.e. 81) is close to the interval while the second value (i.e. 256) is within this interval. For the adhesive

Table 2. Initial values of the radius, length and adhesive force for the ideal-self-similar hierarchical model.

	$\nu = 0.3$	$\nu = 0.35$
$R_0(n\text{m})$	70	72.59
$L_0(n\text{m})$	67.3	80.25
$F_0(n\text{N})$	307.7	330.9

Table 3. Comparison of the predicted structural parameters and adhesive force with the observations of Tokay gecko's seta.

	Predicted			
	$\nu = 0.3$, $m = 3$	$\nu = 0.35$, $m = 3$	$\nu = 0.35$, $m = 4$	Observed
N	4	4	4	4*[33]
$R_N(\mu\text{m})$	2.121	3.342	3.342	~2.5[6,7,12]
M_N	81	81	256	100 ~ 1000[11,12,34]
$F_N(\mu\text{N})$	24.93	26.8	84.71	20 ~ 200[11,13]

*The value is re-evaluated for the multilevel projective terminal of gecko seta based on the reference. In the re-evaluation, spatula is regarded as level 0 and therefore not counted.

force, the predicted values from the present model are 24.93μN, 26.8μN or 84.71μN for different cases. Compared with 20 ~ 200μN,[11,13] they all agree well with the observed interval.

On the whole, the present model can well interpret the fine structure, as well as the large adhesive force of seta.

4. Discussion

4.1. *On the failure mode due to the flaw tolerant adhesion*

In this paper, the robust adhesion of seta is characterized by the flaw tolerant adhesion, based on which the derivations are carried out for the present model. However, with the adhesion ability is enhanced by introducing a hierarchical structure, failure may be caused by fiber fracture at a certain level instead of detachment, i.e. adhesion failure, so that the current robust adhesion loses its significance. In other words, whether fiber fracture takes place at each level is of great importance for the present model.

Consider a single fiber at level n with a penny-shaped crack in the center of the cross-section, which is taken to be a potential internal flaw. For a crack with a half size of fiber, the maximum tensile strength of this fiber can sustain is[23]

$$\sigma_n^f = 1.63\sqrt{\frac{E_n^f \Gamma_f}{(1-\nu_f^2)R_n^f}}, \tag{24}$$

where Γ_f is the fracture energy of fiber, ν_f is the Poisson's ratio of fiber, E_n^f and R_n^f are the Young's modulus and radius of a single fiber at level n. The primary failure mode will be the adhesion failure if $\sigma_n^f > S_n^f$, but the fiber fracture if $\sigma_n^f < S_n^f$, where S_n^f is the adhesion strength of a single fiber at level n. It should be noted that due to the consideration of a single fiber of each level in Equation (24), we have $E_n^f = E_{n-1}$, $R_n^f = R_{n-1}$ and $S_n^f = S_{n-1}$ related to the present model. For Tokay gecko's seta, we have $\Gamma_f = 5\mathrm{J/m}^2$ and $\nu_f = 0.3$,[23] and σ_n^f is then calculated and compared with S_n^f, as shown in Figure 5. It is seen that σ_n^f is always larger than S_n^f with an increasing number of levels. Thus, fiber fracture does not take place at any level, and the adhesion failure is always the primary failure mode for each level.

4.2. *The role of structural hierarchy to the adhesion release*

It is well known that the key feature of gecko seta is its robust attachment and easy detachment. Yao and Gao[23] proposed an anisotropic material model to explain the switch between attachment and detachment by shifting the pulling angle along the longitudinal direction θ of the anisotropic material (corresponding to the

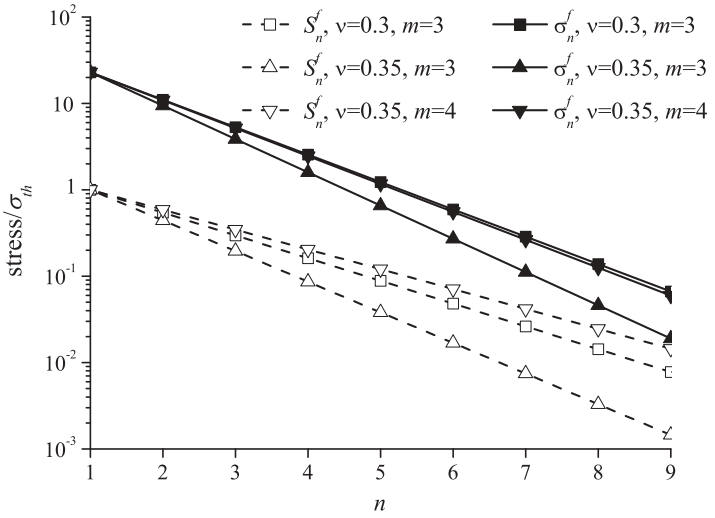

Figure 5. Comparison of the maximum tensile strength σ_n^f with the adhesion strength S_n^f of a single fiber at level n.

maximum pull-off stresses/adhesion strength) and the orientation $(\theta/2 + \pi/2)$ (corresponding to the minimum pull-off stresses/adhesion strength).

In the present model, each level is composed of a fiber array which is anisotropic in the longitudinal and lateral directions. Thus, the orientation dependent pull-off stress/adhesion strength of the anisotropic material model[23] is applicable to the present model. Due to the linear dependence of the adhesive force on S_n in Equation (21), the corresponding orientation dependent adhesive force is accordingly generated at each level. Thus, the structural hierarchy in the present model can retain this advantageous adhesion release.

4.3. *Hierarchy ending of gecko seta*

For gecko seta, the hierarchy ends at the micron-scale.[6,7,12] In our opinion, relative to the foot size, this is probably because the flaw tolerant adhesion at this scale is sufficient for the survival environment of gecko. On the other hand, the hierarchy will be over 10 levels if the dimension arrives at the macro-scale by using the present model. Apparently, the structure becomes terribly complicated at that moment. Therefore, more levels are not necessarily better in practice though having a better flaw tolerant adhesion.

On the whole, hierarchy ending of gecko seta can be understood as a balance of survival environment, foot size and structural complexity for gecko.

5. Conclusions

In this paper, we propose an ideal-self-similar hierarchical model to mimic the multilevel projective terminal of gecko seta. To further construct this model, the

characteristic size and conjugated length to achieve the flaw tolerant adhesion are introduced, and the material properties (including the Young's modulus, adhesion strength and work of adhesion) at each level are evaluated in an effective sense. Variations of the properties in the ideal-self-similar hierarchical model at different levels are examined. Taking Tokay gecko's seta as example, the total number of levels is first evaluated, and the radius, total number of terminal fibers and adhesive force of seta are then predicted. The results from the present model are in agreement with the experimental observations. In addition, the ideal-self-similar hierarchical model can remain the robust adhesion and the advantageous adhesion release at each level.

Nature provides rich sources of inspiration for physical sciences and industrial applications. The present model is beneficial to understand the hierarchical structure and properties of seta and to develop bioinspired environmentally friendly materials in the future. It anticipates that the present model is extended to include the effects of bending,[35,36] tangential contact[37,38] and humidity[39–41] for adhesion biomaterials.

Acknowledgements

This work was supported by the National Natural Science Foundation of China (Grant Nos. 11672221, 11272245). The authors would like to thank the reviewers for their helpful comments and suggestions.

ORCID

Q. K. Zhang http://orcid.org/0000-0002-2434-1614

References

[1] Stork, N. E. A Scanning Electron Microscope Study of Tarsal Adhesive Setae in the Coleoptera. *Zool. J. Linn. Soc.-Lond.* 1980, *68*, 173–306. DOI: 10.1111/j.1096-3642.1980.tb01121.x.

[2] Stork, N. E. A Comparison of the Adhesive Setae on the Feet of Lizards and Arthropods. *J. Nat. Hist.* 1983, *17*, 829–835. DOI: 10.1080/00222938300770641.

[3] Beutel, R. G.; Gorb, S. N. Ultrastructure of Attachment Specializations of Hexapods (Arthropoda): Evolutionary Patterns Inferred from a Revised Ordinal Phylogeny. *J. Zool. Syst. Evol. Res.* 2001, *39*, 177–207. DOI: 10.1046/j.1439-0469.2001.00155.x.

[4] Kesel, A. B.; Martin, A.; Seidl, T. Adhesion Measurements on the Attachment Devices of the Jumping Spider Evarcha Arcuata. *J. Exp. Biol.* 2003, *206*, 2733–2738. DOI: 10.1242/jeb.00478.

[5] Scherge, M.; Gorb, S. Biological Frictional and Adhesive Systems. *Biological Micro- and Nanotribology: Nature's Solutions*; Springer: Berlin, Heidelberg, 2001; pp 79–127. DOI:10.1007/978-3-662-04431-5_3.

[6] Ruibal, R.; Ernst, V. The Structure of the Digital Setae of Lizards. *J. Morphol.* 1965, *117*, 271–294. DOI: 10.1002/jmor.1051170302.

[7] Russell, A. P. A Contribution to the Functional Analysis of the Foot of the Tokay, *Gekko Gecko* (Reptilia: Gekkonidae). *J. Zool. (London)*. 1975, *176*, 437–476. DOI: 10.1111/j.1469-7998.1975.tb03215.x.
[8] Arzt, E.; Gorb, S.; Spolenak, R. From Micro to Nano Contacts in Biological Attachment Devices. *Proc. Natl. Acad. Sci. USA*. 2003, *100*, 10603–10606. DOI: 10.1073/pnas.1534701100.
[9] Autumn, K.; Dittmore, A.; Santos, D.; Spenko, M.; Cutkosky, M. Frictional Adhesion: A New Angle on Gecko Attachment. *J. Exp. Biol.* 2006, *209*, 3569–3579. DOI: 10.1242/jeb.02486.
[10] Yao, H. M.; Gao, H. J. Multi-Scale Cohesive Laws in Hierarchical Materials. *Int. J. Solids. Struct.* 2007, *44*, 8177–8193. DOI: 10.1016/j.ijsolstr.2007.06.007.
[11] Autumn, K.; Liang, Y. C.; Hsieh, S. T.; Zesch, W.; Chan, W. P.; Kenny, T.; Fearing, R.; Full, R. J. Adhesive Force of a Single Gecko Foot-Hair. *Nature*. 2000, *405*, 681–685. DOI: 10.1038/35015073.
[12] Autumn, K.; Peattie, A. M. Mechanisms of Adhesion in Geckos. *Integr. Comp. Biol.* 2002, *42*, 1081–1090. DOI: 10.1093/icb/42.6.1081.
[13] Autumn, K.; Sitti, M.; Liang, Y. A.; Peattie, A. M.; Hansen, W. R.; Sponberg, S.; Kenny, T. W.; Fearing, R.; Isrealachvili, J. N.; Full, R. J. Evidence for Van Der Waals Adhesion in Gecko Setae. *Proc. Natl. Acad. Sci. USA*. 2002, *99*, 12252–12256. DOI: 10.1073/pnas.192252799.
[14] Gao, H. J.; Yao, H. M. Shape Insensitive Optimal Adhesion of Nanoscale Fibrillar Structures. *Proc. Natl. Acad. Sci. USA*. 2004, *101*, 7851–7856. DOI: 10.1073/pnas.0400757101.
[15] Pesika, N. S.; Zhao, B. X.; Rosenberg, K.; Zeng, H. B.; McGuiggan, P.; Autumn, K.; Israelachvili, J. N. Peel-Zone Model of Tape Peeling Based on the Gecko Adhesive System. *J. Adhes.* 2007, *83*, 383–401. DOI: 10.1080/00218460701282539.
[16] Gao, H. J.; Wang, X.; Yao, H. M.; Gorb, S. ; Arzt, E. Mechanics of Hierarchical Adhesion Structures of Geckos. *Mech. Mater.* 2005, *37*, 275–285. DOI: 10.1016/j.mechmat.2004.03.008.
[17] Endoh, K. S.; Kawakatsu, T.; Müller-Plathe, F. Coarse-Grained Molecular Simulation Model for Gecko Feet Keratin. *J. Phys. Chem. B*. 2018, *122*, 2203–2212. DOI: 10.1021/acs.jpcb.7b10481.
[18] Jagota, A.; Bennison, S. J. Mechanics of Adhesion through a Fibrillar Microstructure. *Integr. Comp. Biol.* 2002, *42*, 1140–1145. DOI: 10.1093/icb/42.6.1140.
[19] Persson, B. N. J. On the Mechanism of Adhesion in Biological Systems. *J. Chem. Phys.* 2003, *118*, 7614–7621. DOI: 10.1063/1.1562192.
[20] Hagey, T. J.; Puthoff, J. H.; Holbrook, M.; Harmon, L. J.; Autumn, K. Variation in Setal Micromechanics and Performance of Two Gecko Species. *Zoomorphology*. 2014, *133*, 111–126. DOI: 10.1007/s00435-013-0207-2.
[21] Chen, B.; Wu, P. D.; Gao, H. J. Hierarchical Modelling of Attachment and Detachment Mechanisms of Gecko Toe Adhesion. *Proc. R. Soc. A*. 2008, *464*,1639–1652. DOI: 10.2307/20209488.
[22] Wu, X.; Wang, X. J.; Mei, T.; Sun, S. M. Mechanical Analyses on the Digital Behaviour of the Tokay Gecko (*Gekko Gecko*) Based on a Multi-Level Directional Adhesion Model. *Proc. R. Soc. A*. 2015, *471*, 20150085. DOI: 10.1098/rspa.2015.0085.
[23] Yao, H. M.; Gao, H. J. Mechanics of Robust and Releasable Adhesion in Biology: Bottom–Up Designed Hierarchical Structures of Gecko. *J. Mech. Phys. Solids*. 2006, *54*, 1120–1146. DOI: 10.1016/j.jmps.2006.01.002.
[24] Kim, T. W.; Bhushan, B. Adhesion Analysis of Multi-Level Hierarchical Attachment System Contacting with a Rough Surface. *J. Adhes. Sci. Technol.* 2007, *21*, 1–20. DOI: 10.1163/156856107779976097.

[25] Sauer, R. A. Multiscale Modeling and Simulation of the Deformation and Adhesion of a Single Gecko Seta. *Comp. Meth. Biomech. Biomed. Eng.* 2009, *12*, 627–640. DOI: 10.1080/10255840902802917.

[26] Sauer, R. A. A Computational Model for Nanoscale Adhesion between Deformable Solids and Its Application to Gecko Adhesion. *J. Adhes. Sci. Technol.* 2010, *24*, 1807–1818. DOI: 10.1163/016942410X507588.

[27] Schleich, H. H.; Kästle, W. Ultrastrukturen an Gecko-Zehen (Reptilia: Sauria: Gekkonidae). *Amphibia Reptilia*. 1986, *7*, 141–166. DOI: 10.1163/156853886X00361.

[28] Gao, H. J.; Chen, S. H. Flaw Tolerance in a Thin Strip under Tension. *J. Appl. Mech.* 2005, *72*, 732–737. DOI: 10.1115/1.1988348.

[29] Yao, H. M. Mechanics of Robust and Releasable Adhesion in Biology. Ph.D. Dissertation, Stuttgart University, Stuttgart, Germany, 2006. DOI: 10.18419/opus-6617.

[30] Hu, C.; Greaney, P. A. Role of Seta Angle and Flexibility in the Gecko Adhesion Mechanism. *J. Appl. Phys.* 2014, *116*, 074302. DOI: 10.1063/1.4892628.

[31] Sekiguchi, Y.; Saito, S.; Takahashi, K.; Sato, C. Flexibility and Poisson Effect on Detachment of Gecko-Inspired Adhesives. *Int. J. Adhes. Adhes.* 2015, *62*, 55–62. DOI: 10.1016/j.ijadhadh.2015.06.011.

[32] Sekiguchi, Y.; Takahashi, K.; Sato, C. Adhesion Mechanism of a Gecko-Inspired Oblique Structure with an Adhesive Tip for Asymmetric Detachment. *J. Phys. D: Appl. Phys.* 2015, *48*, 475301. DOI: 10.1088/0022-3727/48/47/475301.

[33] Tang, Y. Z. The Secret of Gecko Toe. *China Nat.* 2013, *5*, 32–34 (in Chinese). DOI: 10.3969/j.issn.0255-7800.2013.05.010.

[34] Tian, Y.; Pesika, N.; Zeng, H.; Rosenberg, K.; Zhao, B. X.; McGuiggan, P.; Autumn, K.; Israelachvili, J. Adhesion and Friction in Gecko Toe Attachment and Detachment. *Proc. Natl. Acad. Sci. USA*. 2006, *103*, 19320–19325. DOI: 10.1073/pnas.0608841103.

[35] Persson, B. N. J.; Gorb, S. The Effect of Surface Roughness on the Adhesion of Elastic Plates with Applications to Biological Systems. *J. Chem. Phys.* 2003, *119*, 11437–11444. DOI: 10.1063/1.1621854.

[36] Gravish, N.; Wilkinson, M.; Autumn, K. Frictional and Elastic Energy in Gecko Adhesive Detachment. *J. R. Soc. Interface*. 2008, *5*, 339–348. DOI: 10.1098/rsif.2007.1077.

[37] Glassmaker, N. J.; Jagota, A.; Hui, C. Y.; Kim, J. Design of Biomimetic Fibrillar Interfaces: 1. Making Contact. *J. R. Soc. Interface*. 2004, *1*, 23–33. DOI: 10.1098/rsif.2004.0004.

[38] Kim, T. W.; Bhushan, B. The Adhesion Model considering Capillarity for Gecko Attachment System. *J. R. Soc. Interface*. 2007, *5*, 319–327. DOI: 10.1098/rsif.2007.1078.

[39] Puthoff, J. B.; Prowse, M. S.; Wilkinson, M.; Autumn, K. Changes in Materials Properties Explain the Effects of Humidity on Gecko Adhesion. *J. Exp. Biol.* 2010, *213*, 3699–3704. DOI: 10.1242/jeb.047654.

[40] Prowse, M. S.; Wilkinson, M.; Puthoff, J. B.; Mayer, J.; Autumn, K. Effects of Humidity on the Mechanical Properties of Gecko Setae. *Acta Biomater.* 2011, *7*, 733–738. DOI: 10.1016/j.actbio.2010.09.036.

[41] Tao, D.; Wan, J.; Pesika, N. S.; Zeng, H.; Liu, Z.; Zhang, X.; Meng, Y.; Tian, Y. Adhesion and Friction of an Isolated Gecko Setal Array: The Effects of Substrates and Relative Humidity. *Biosurf. Biotribol.* 2015, *1*, 42–49. DOI: 10.1016/j.bsbt.2015.02.002.

Appendix A. Derivation of the conjugate characteristic length based on flaw tolerant adhesion

To derivate the conjugate characteristic length, we consider an elastic plate with flaw tolerant adhesion adhering to a rigid substrate, as shown in Figure 6a. An interfacial crack of size a is used to simulate the random contact flaws along the interface. At this situation, the stress outside the crack uniformly reaches the theoretical strength S at the critical state of pull-off, while the crack tip separation δ_{tip} stays within the adhesive interaction range (Figure 6b). Our goal is to search for the characteristic length L conjugating to the characteristic size (half-width) of the plate. Physically, this problem can be simplified by superposing a uniform pressure equal to S on the entire surface, as shown in Figure 6c. Thus, the solution to the problem of Figure 6a is converted to an elastic plate subjected to uniform pressure S over $x \leq a$, as shown in Figure 6d, so that the crack tip separation δ_{tip} in Figure 6b is equal to the surface displacement at $x = a$ relative to a surface point at infinity in Figure 6d.[29]

Due to symmetry, the displacement field in the vicinity of $x = 0$ has only one non-zero displacement component u_y dependent on y, leading to one non-zero strain component ε_{yy}. Under this circumstance, the equilibrium equation is reduced to

$$\frac{\partial \sigma_{yy}}{\partial y} = 0. \tag{A1}$$

Considering the boundary condition $\sigma_{yy}\big|_{y=0} = -S$, Equation (A1) yields

$$\sigma_{yy} = -S. \tag{A2}$$

On the other hand, from the elasticity theory, we have

$$\sigma_{yy} = \frac{E(1-\nu)\varepsilon_{yy}}{(1+\nu)(1-2\nu)}. \tag{A3}$$

From Equations (A2) and (A3), we obtain

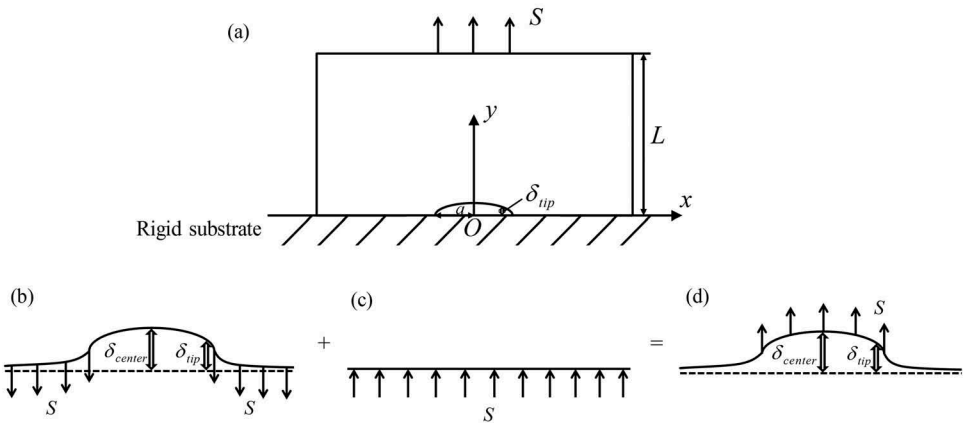

Figure 6. Flaw tolerant adhesion of the plate: (a) An elastic plate with flaw tolerant adhesion is in contact with a rigid substrate. (b) The corresponding state of stress distribution: the adhesive stress outside the crack uniformly reaches the theoretical strength S of the plate with no stress concentration near the crack tip. (c) By superposing a uniform pressure of S on the entire surface, (d) the equivalent problem of the flaw tolerant adhesion is converted into an elastic plate subjected to a uniform pressure over a circular area.

$$\varepsilon_{yy} = -\frac{(1+\nu)(1-2\nu)S}{E(1-\nu)}. \tag{A4}$$

Therefore, the surface deflection at the center of the pressurized region ($x = 0$, $y = 0$) in Figure 6d is

$$\delta_{center} = \frac{(1+\nu)(1-2\nu)SL}{E(1-\nu)}. \tag{A5}$$

For simplicity, we assume that the relation of $\lim_{a\to\infty} \delta_{tip} = \frac{1}{2}\lim_{a\to\infty} \delta_{center}$ (δ_{tip} is the crack tip opening displacement) for the infinite flaw[29] is still applicable for a finite flaw, and then, we obtain

$$\delta_{tip} = \frac{1}{2}\delta_{center} = \frac{(1+\nu)(1-2\nu)SL}{2(1-\nu)E}. \tag{A6}$$

Meanwhile, the condition to achieve flaw tolerant adhesion is that δ_{tip} stays within the adhesive interaction range. According to Dugdale model, we have

$$\delta_{tip} \le \delta_{cr} = \frac{W}{S}, \tag{A7}$$

where δ_{cr} is the critical crack tip opening displacement.
From Equation (A7), Equation (A6) yields a condition as

$$L \le L_{cr} = \frac{2(1-\nu)EW}{(1+\nu)(1-2\nu)S^2}, \tag{A8}$$

where L is the conjugate characteristic length to be sought.

Appendix B. Requirement for the number of fibers in a fiber array

Here, for the placement of fibers, the regular lattice patterns are studied to obtain the requirement for the number of fibers in a fiber array. As explained in Section 2.1, the number of fibers is a single digit for each level, thus, the regular lattice pattern is an m-polygonal lattice. To achievement, we divide the cross-section with radius R_n into m equal sectors, and then, placing a cross-section with radius R_{n-1} at the symmetric location of each sector.

As shown in Figure 7, for the sector with the central angle of $2\pi/m$, and denoting the distance between the centers of two cross-sections (i.e. R_n and R_{n-1}) by d, the complete placement of a cross-section with radius R_{n-1} in this sector requires

$$d + R_{n-1} \le R_n \tag{B1}$$

and

$$d\sin(\pi/m) \ge R_{n-1}. \tag{B2}$$

With Equation (12), we can immediately obtain

$$m \le \pi/\arcsin(\frac{1}{c_1 - 1}) \tag{B3}$$

from Equations (B1) and (B2).
In practice, the regular lattice pattern is triangular at least. So, Equation (B3) is further extended to be

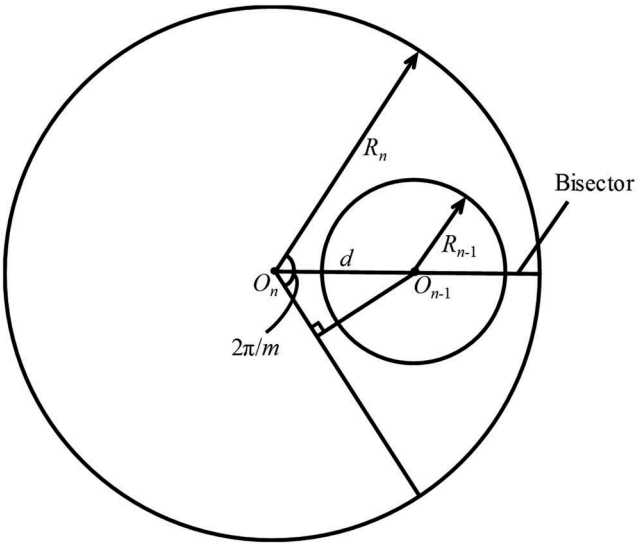

Figure 7. The geometric relation if m cross-sections with radius R_{n-1} are placed in a cross-section with radius R_n for the regular lattice pattern.

$$3 \leq m \leq \pi/\arcsin\left(\frac{1}{c_1 - 1}\right). \tag{B4}$$

Equation (B4) is the requirement for the number of fibers in a fiber array. With this requirement, the structural constant (i.e. c_1) must fulfill

$$c_1 \geq 2.154. \tag{B5}$$